Since January 2020 Elsevier has created a COVID-19 resource centre with free information in English and Mandarin on the novel coronavirus COVID-19. The COVID-19 resource centre is hosted on Elsevier Connect, the company's public news and information website.

Free Radical Biology and Medicine 191 (2022) 105–118

Contents lists available at ScienceDirect

Free Radical Biology and Medicine

journal homepage: www.elsevier.com/locate/freeradbiomed

Toxicity and virucidal activity of a neon-driven micro plasma jet on eukaryotic cells and a coronavirus

Daniel M. Mrochen [a], Lea Miebach [a,b], Henry Skowski [a], Robert Bansemer [a], Chiara A. Drechsler [a,c], Ulfilas Hoffmann [a], Manuel Hein [d], Uwe Mamat [d,f], Torsten Gerling [a], Ulrich Schaible [d,f,g], Thomas von Woedtke [a,e,g,1], Sander Bekeschus [a,g,1,*]

[a] ZIK plasmatis, Leibniz Institute for Plasma Science and Technology (INP), Felix-Hausdorff-Str. 2, 17489, Greifswald, Germany
[b] Department of General, Visceral, Vascular, and Thoracic Surgery, Greifswald University Medical Center, Ferdinand-Sauerbruch-Str., 17475, Greifswald, Germany
[c] Department of Obstetrics and Gynecology, Greifswald University Medical Center, Ferdinand-Sauerbruch-Str., 17475, Greifswald, Germany
[d] Department of Cellular Microbiology, Program Area Infections, Research Center Borstel, Leibniz Lung Center, Parkallee, 23845, Borstel, Germany
[e] Institute for Hygiene and Environmental Medicine, Greifswald University Medical Center, Ferdinand-Sauerbruch-Str., 17475, Greifswald, Germany
[f] Leibniz Research Alliance INFECTIONS, Germany
[g] Leibniz Research Alliance HEALTH TECHNOLOGIES, Germany

ARTICLE INFO

Keywords:
Cold physical plasma
Gas plasma technology
MHV
Murine hepatitis virus
Virus inactivation
Reactive oxygen species
ROS

ABSTRACT

Plasma medicine is a developing field that utilizes the effects of cold physical plasma on biological substrates for therapeutic purposes. Approved plasma technology is frequently used in clinics to treat chronic wounds and skin infections. One mode of action responsible for beneficial effects in patients is the potent antimicrobial activity of cold plasma systems, which is linked to their unique generation of a plethora of reactive oxygen and nitrogen species (ROS). During the SARS-CoV-2 pandemic, it became increasingly clear that societies need novel ways of passive and active protection from viral airway infections. Plasma technology may be suitable for superficial virus inactivation. Employing an optimized neon-driven micro plasma jet, treatment time-dependent ROS production and cytotoxic effects to different degrees were found in four different human cell lines with respect to their metabolic activity and viability. Using the murine hepatitis virus (MHV), a taxonomic relative of human coronaviruses, plasma exposure drastically reduced the number of infected murine fibroblasts by up to 3000-fold. Direct plasma contact (conductive) with the target maximized ROS production, cytotoxicity, and antiviral activity compared to non-conductive treatment with the remote gas phase only. Strikingly, antioxidant pretreatment reduced but not abrogated conductive plasma exposure effects, pointing to potential non-ROS-related mechanisms of antiviral activity. In summary, an optimized micro plasma jet showed antiviral activity and cytotoxicity in human cells, which was in part ROS-dependent. Further studies using more complex tissue models are needed to identify a safe dose-effect window of antiviral activity at modest toxicity.

1. Introduction

The SARS-CoV-2 pandemic has highlighted the severe threat emerging respiratory viruses pose to humans [1]. Effective ways to prevent infection and treat infected individuals are urgently needed to address this threat. Methods to prevent infection primarily rely on behavioral changes and hygiene measures by those affected, such as keeping distance from others up to quarantine, wearing appropriate masks, and frequent disinfection [2]. Especially indoors, it has been shown that the viral load in the form of aerosolized droplets can be reduced by filtration and physical inactivation, e.g., by UV light or reactive oxygen species such as ozone [3–5]. Therefore, cold plasma, as a source of not only UV light and reactive oxygen species, gains increasing attention for virus inactivation both in the environment and in humans [6–9].

In the emerging field of plasma medicine, cold physical plasma has already established itself as an effective means for various experimental and clinical therapeutic purposes. Cold plasma is an energetic and

* Corresponding author. ZIK plasmatis, Leibniz Institute for Plasma Science and Technology (INP), Felix-Hausdorff-Str. 2, 17489, Greifswald, Germany.
E-mail address: sander.bekeschus@inp-greifswald.de (S. Bekeschus).
[1] contributed equally as last authors.

https://doi.org/10.1016/j.freeradbiomed.2022.08.026
Received 22 April 2022; Received in revised form 6 August 2022; Accepted 15 August 2022
Available online 28 August 2022

partially ionized gas. It contains ions and mobile electrons in an electric field, emits electromagnetic radiation such as UV, visible and infrared light, and causes the formation of reactive oxygen and nitrogen species (hereafter referred to as ROS) through interactions with ambient air reaction partners such as oxygen and nitrogen [10]. The quality and quantity of the different plasma components, including the individual reactive species generated, differ to a certain degree depending on the type of plasma source and its geometry as well as feed gas and operating voltage used. Notwithstanding, overall similar biological effects of cold plasma have been described [11]. As part of hygiene solutions, cold plasma has been described for disinfecting medical equipment and goods in food processing [12,13]. In the clinical setting, approved plasma technology is used to treat chronic wounds [14]. The applications in wound healing and for disinfection purposes are based on the finding that the cold plasma-derived ROS have been ascribed potent antimicrobial properties [15,16], which comes as no surprise considering ROS being an integral part of the innate immune defense against microorganisms. Although the potential antiviral activity of cold plasma has been addressed in several studies [7,8,17], much more needs to be learned regarding the efficacy of different plasma sources, treatment modalities and to untangle the precise mechanisms of action.

To this end, this study investigated the toxicity and antiviral activity

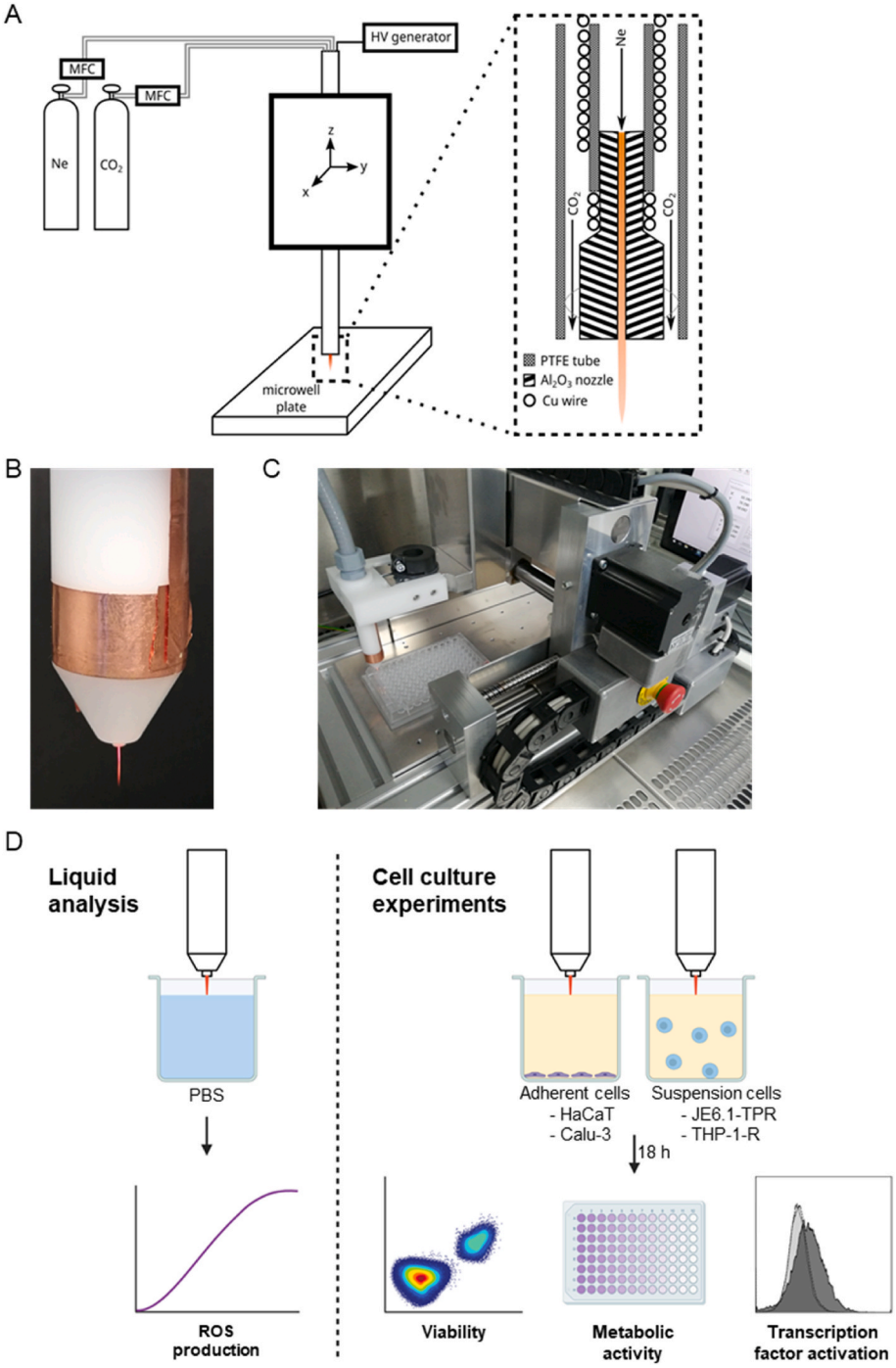

Fig. 1. Experimental plasma setup. (A) Scheme of the miniaturized neon plasma jet mounted in an *xyz*-stage, and technical drawing of the plasma jet head (right). (B) Photo of the micro plasma jet device and plasma effluent. (C) Photo of the micro plasma jet device attached to the *xyz*-stage. (D) Experimental setup for liquid analyses and cell experiments. MFC: mass flow controller; HV: high voltage; PTFE: polytetrafluoroethylene.

of a neon-driven micro plasma jet. Cytotoxic effects and transcription factor activity were studied in four human cell lines using different plasma treatment modes. Moreover, the murine hepatitis virus (MHV) was used as a coronavirus model, and its inactivation by cold plasma was measured. The results show apparent effects of plasma exposure on both cell survival and virus inactivation at similar treatment times, indicating potential applications of the micro plasma jet provided that optimal treatment time intensities windows are identified.

2. Materials and methods

2.1. Plasma source and treatment

Cold physical plasma was produced using a miniaturized neon plasma jet described and characterized before [18,19]. Three hundred sccm neon (Ne) were used as feed gas and shielded with 300 sccm carbon dioxide (CO_2). The plasma jet head consists of an aluminum oxide (Al_2O_3) ceramic nozzle that forms a 0.6 mm wide capillary (Fig. 1A) in which a Ne plasma is ignited (Fig. 1B). The electric field necessary for the ignition is provided by a copper wire wound around a part of the nozzle. It carries a sinusoidal high-voltage signal with a frequency of approximately 415 kHz that is periodically switched on and off in a 1 kHz cycle, in which it is 32% of the time switched on and 68% of the time switched off. An approximately 5 mm long visible effluent protruding from the nozzle is generated with these operating parameters. If the treatment target is located within this distance of about 5 mm, the effluent visibly connects to the target, and, as the target acts as a counter electrode, the discharge becomes slightly more intense and brighter. The discharge then forms a conductive channel towards the treatment target. In contrast to this conductive mode, the jet can be used to treat targets remotely without any connection, referred to as non-conductive, as described before [20]. A programmable *xyz*-stage (CNC, Germany) was used to treat liquids, cell suspensions, and virus suspensions in a pre-defined and automated fashion at 10 μm-precision to ensure comparable treatment conditions over time (Fig. 1C). If not indicated otherwise, plasma treatments were performed in conductive mode targeting a liquid with a volume of 300 μL in 96-well flat-bottom plates (Sarstedt, Germany) with the jet nozzle placed 3 mm over the liquid surface. In non-conductive mode, the distance was 7 mm or 11 mm. A predetermined amount of double-distilled water was added for each plasma treatment time to compensate for evaporation.

2.2. Quantification of reactive oxygen and nitrogen species

Relative detection of short-lived ROS deposition in liquids was done using singlet oxygen sensor (SOS; Thermo Scientific, Germany) indicative of singlet oxygen ($^1O_2$), hydroxyphenyl fluorescein (HPF; Enzo, Germany) indicative of peroxynitrite ($ONOO^-$) and hydroxyl radicals ($^{\cdot}OH$) and aminophenyl fluorescein (APF; Enzo, Germany) indicative of $ONOO^-$, $^{\cdot}OH$ and hypochlorous acid (HOCl). Fluorescent redox probes were added to PBS or R2F prior treatment at a concentration of 20 μM, respectively. Liquids were exposed to plasma in 96-well flat-bottom plates at a volume of 300 μL per well for 10, 20, and 30 s in conductive mode. Specificity for detection of short-lived species was verified by addition of 5 μg/mL catalase (cat) prior to plasma treatment or by measurement of 50 μM-solutions of H_2O_2. For all probes, fluorescence was determined at λ_{ex} 485 nm and λ_{em} 525 nm in a microplate reader (F200; Tecan, Switzerland). Scavenging activity of selected molecules was done following similar conditions. Briefly, ascorbic acid (200 μM; AA), cysteine (1 mM), DMSO (1 mM), glutathione (2 mM), histidine (1 mM), mannitol (1 mM), tyrosine (1 mM), N-acetylcysteine (10 mM; NAC) and trolox (50 μM; all Sigma Aldrich, Germany) were added to PBS or R2F and exposed to plasma for 30 s immediately after. Scavenging activity was calculated as percent fluorescent intensity reduction compared to untreated controls without scavengers. Untreated, scavenger-containing controls were used for background subtraction of corresponding plasma-treated samples. Generation of hydrogen peroxide (H_2O_2) in plasma-treated liquids was quantified using the Amplex Ultra Red assay (Thermo Fisher Scientific, Germany), as described before [20]. The amount of nitrite (NO_2^-) and nitrate (NO_3^-) in plasma-treated liquids was determined using the Griess assay (Cayman Chemical, Germany) according to the manufacturer's instructions (Fig. 1D). Technical replicates were treated consecutively, one after another.

2.3. Cell culture

JE6.1-triple parameter reporters (JE6.1-TPR: NFκB:eCFP, NFAT:eGFP, AP-1:mCherry), a recombinant lymphocytic cell line originating from Jurkat cells, and THP-1-NFκB:eGFP-TLR4-CD14 (THP-1-R), a monocytic cell line, were provided by Peter Steinberger (Medical University of Vienna, Austria) [21,22]. JE6.1-TPR and THP-1-R were maintained in cell culture flasks in R10F, consisting of Roswell Park Memorial Institute 1640 (RPMI1640) cell culture medium supplemented with 10% fetal calf serum (FCS), 2 mM glutamine, 100 U/mL penicillin, and 0.1 mg/mL streptomycin (PAN-Biotech, Germany). Prior to plasma treatment, cells were harvested and washed with PBS, and 2×10^4 cells per well were seeded in fresh R10F in 96-well flat-bottom plates. Plasma treatment took place within 30 min after seeding the cells. If indicated, 10 mM of the ROS-scavenging agent NAC and/or 5 μg/mL catalase were added immediately before plasma treatment. The human lung adenocarcinoma Calu-3 cell line (HTB-55) was obtained from ATCC and was maintained in cell culture flasks in R10F. HaCaT cells, spontaneously immortalized, non-tumorigenic human keratinocytes, were maintained in cell culture flasks in DMEM10, consisting of Dulbecco's Modified Eagle Medium (DMEM) supplemented with 10% FCS, 2 mM glutamine, 100 U/mL penicillin, and 0.1 mg/mL streptomycin. Cells were harvested with Accutase cell detachment solution (BioLegend, The Netherlands) and washed with PBS. A total of 1×10^4 HaCaT cells or 2×10^4 Calu-3 cells per well were seeded in fresh R10F in 96-well flat-bottom plates and allowed to adhere in an incubator (37 °C, 5% CO_2, 95% humidity) for 18 h. Before plasma treatment, cells were washed with PBS, and fresh R10F was added. If indicated, 10 mM of NAC and/or 5 μg/mL catalase were added immediately before plasma treatment (Fig. 1D).

2.4. Metabolic activity

To analyze metabolic activity 18 h after plasma treatment, 100 μL of cell culture medium was replaced with R10F containing resazurin (Sigma, Germany) so that the final concentration in the wells was at 100 μM. Resazurin diffuses freely into cells and is reduced to its fluorescent product, resorufin, as a function of the cell's metabolic activity. After 4 h of incubation, the plate was transferred to microplate reader (F200; Tecan, Switzerland), and resorufin fluorescence was quantified at λ_{ex} 535 nm and λ_{em} 590 nm.

2.5. Measurement of calcium effects

To measure the calcium flux after plasma treatment, TK6 cells were loaded with Fluo-3-AM (Thermo Fisher Scientific, Germany) for 15 min according to the manufacturer's instructions. JE6.1-TPR were not used for this experiment because their reporter signal would have interfered with the calcium-induced Fluo-3 signal. Afterward, cells were resuspended in DMEM10 and treated with the micro plasma jet for exposure various times. PMA (20 ng/mL) and Ionomycin (1 μg/mL) were used as a positive control. 10 min or 1 h after plasma treatment the Fluo-3 signal was measured using flow cytometry (CytoFLEX S; Beckman-Coulter, Germany), and data analysis was performed using Kaluza analysis software 2.1.3 (Beckman-Coulter, Germany). To analyze the impact of calcium on the activation of the transcription factor NFAT in JE6.1-TPR, cells were loaded with the calcium chelator BAPTA-AM (Thermo Fisher Scientific, Germany) according to the manufacturer's instructions before

plasma treatment. 18 h after plasma treatment, the activation of NFAT was measured by its reporter signal using flow cytometry.

2.6. Cell viability

If not indicated otherwise, cell viability was determined 18 h after plasma treatment by staining with Annexin V and DAPI (4′,6-Diamidino-2-phenylindole) or Zombie NIR (all BioLegend, The Netherlands). After incubation, cells were harvested either with (HaCaT, Calu-3) or without (JE6.1-TPR, THP-1-R) Accutase. Care was taken to include cells in the supernatant of adherent cells (HaCaT, Calu-3) to avoid missing dying or dead cells that had already lost adhesion. Afterward, cells were washed with Annexin V Binding Buffer (BioLegend, The Netherlands) and stained with either Annexin V (Alexa Fluor 647) and DAPI (1 μM) (HaCaT, Calu-3), Annexin V (PE) and DAPI (1 μM) (THP-1-R), or Annexin V (Alexa Fluor 647) and Zombie NIR (JE6.1-TPR). Cells were measured using flow cytometry (CytoFLEX LX; Beckman-Coulter, Germany), and data analysis was performed using Kaluza analysis software 2.1.3 (Beckman-Coulter, Germany). Viable cells were defined as Annexin V^- and Zombie NIR^- or $DAPI^-$.

2.7. Preparation of viral stocks

17Cl-1 cells, a murine fibroblast cell line, and MHV-A59-GFP reporter virus (MHV), a murine coronavirus, were provided by Volker Thiel (University Bern, Switzerland). 17Cl-1 cells were maintained in cell culture flasks in DMEM10 (37 °C, 5% CO_2, 95% humidity) and grown to 90% confluency for viral amplification. A modified protocol from Leibowitz et al. was used [23]. Before infection, cells were washed with PBS and then infected with MHV (multiplicity of infection: 0.01) in R2F consisting of RPMI1640 supplemented with 2% FCS, 2 mM glutamine, 100 U/mL penicillin, and 0.1 mg/mL streptomycin. After 2 h, cells were washed with PBS, and fresh R2F was added. Cells were cultured for 48 h in an incubator (37 °C, 5% CO_2, 95% humidity), then the cells were subjected to three freeze-thaw cycles to release viruses from cells that had not been lysed already. To remove cellular debris, the lysate was centrifuged at 3000×*g* for 30 min (4 °C). Afterward, the supernatant was filtered through a 0.22 μm filter, aliquoted, and stored at −80 °C.

2.8. Plasma treatment of viruses

Virus stocks were diluted 1:3 in PBS for plasma treatment, and 300 μL per well were transferred to 96-well flat-bottom plates. If indicated, NAC (final concentration: 10 mM), catalase (5 μg/mL), ascorbic acid (25 mM), and/or trolox (1 mM) were added to the PBS. Viral suspensions were treated on the *xyz*-stage to ensure stable and comparable treatment conditions. After compensating for the evaporation-induced volume loss by adding predetermined amounts of double-distilled water, viral suspensions were diluted, and the plaque assay was performed to determine the viral titer. Viral titer was related to untreated virus and expressed as "relative viral titer."

2.9. Plaque assay

A modified plaque assay was used to determine the viral titer after virus amplification and plasma treatment [23]. Briefly, 17Cl-1 cells were grown to 100% confluency in 6-well plates in DMEM10, washed with PBS, and infected for 90 min with 250 μL of diluted virus suspensions in DMEM2 (DMEM supplemented with 2% FCS, 2 mM glutamine, 100 U/mL penicillin and 0.1 mg/mL streptomycin). Triplicates were used for each dilution. In the meantime, a 1.6% (w/v) liquefied agarose type I solution was mixed in equal parts with double-concentrated DMEM2 and stored at 50 °C in a water bath. After incubation, the cells were overlaid with the DMEM2-agar without washing, and the plates were gently swirled while the agar was still liquid to absorb the viral inoculum into it. The plates were left undisturbed at room temperature until the agar had solidified, transferred to an incubator, and incubated for 48 h (37 °C, 5% CO_2, 95% humidity). To visualize the plaques, a 0.33% (w/v) solution of neutral red (Sigma, Germany) was diluted 1:33 in PBS, and 2 mL were added to each well, directly on top of the agar-overlay. After 3 h of incubation at 37 °C, superfluous neutral red solution was discarded, and plaques were counted against a bright background. To determine the viral titer, the following formula was used:

Titer [PFU (plaque-forming units)/mL] = Average plaque count x dilution factor x 4.

2.10. Metabolic activity after viral infection

17Cl-1 cells were grown to 100% confluency in 96-well flat-bottom plates. After plasma treatment, viral suspensions were diluted in R10F, and 100 μL were transferred to six wells per condition and dilution before 15 h of incubation (37 °C, 5% CO_2, 95% humidity). Then, 100 μL of resazurin (200 μM) in R10F was added, and the plate was incubated for 4 h before resorufin fluorescence was quantified at λ_{ex} 535 nm and λ_{em} 590 nm in a microplate reader (F200; Tecan).

2.11. Infrared spectroscopy

Before the temperature measurement, 300 μl of PBS was added to a well of a 96-well flat bottom plate. The gas plasma treatment regimen and distances were calibrated using an *xyz* motorized stage and a 10 μm-precision caliper (Preciva, Germany). An infrared camera (Optris, Germany) was used for the thermographic measurement throughout 2 min of plasma treatment.

2.12. Statistical analysis

Graphing and statistical analysis were performed using Prism 9.4.1 (GraphPad Software, USA) and one-way analysis of variances (ANOVA) or *t*-test as indicated in the figure legends. Data show mean ± standard deviation (S.D.) if not indicated otherwise. Levels of significance were indicated as follows: ns = non-significant, p = 0.05 (*), p = 0.01 (**), p = 0.001 (***), p = 0.0001 (****).

3. Results

3.1. ROS production of plasma-treated liquids was stable

In this study, the micro plasma jet was used (Fig. 1A), emitting a visible plasma effluent of 5 mm (Fig. 1B) that intensified upon contact with a target. For reproducible plasma treatment *in vitro*, the jet was hovered for a predetermined time over the centers of the wells of 96-well plates via a motorized *xyz*-stage in an automated fashion (Fig. 1C). Before performing antiviral studies, our study protocol included the analysis of plasma-derived ROS and toxicity studies in four human cell lines (Fig. 1D). Exposure of liquids to the plasma resulted in a loss of water that must be replenished to maintain iso-osmolarity. Using the plasma in conductive mode (nozzle 3 mm away from the liquid surface), we measured an evaporation rate of about 0.16 μL/s of treatment time (Fig. 2A). The calculated amount of water that had evaporated during the plasma treatment was replenished in each cavity afterward. Humidity accumulating in tubings overnight can affect plasma-derived ROS production [24]. To identify the initial operation time necessary to achieve stable plasma generation and ROS levels, we measured the H_2O_2 production immediately, 15 min or 30 min after switching on the plasma jet. Immediately after plasma ignition, there was a slightly increased production of H_2O_2 compared to its production after 15 min or 30 min of continuous operation, in which H_2O_2 production was overall comparable (Fig. 2B). Therefore, we decided to use a minimum operation time of 15 min before using the device in the subsequent experiments to allow stable plasma generation. Moreover, it was apparent that H_2O_2 production increases with prolonged treatment times. This was

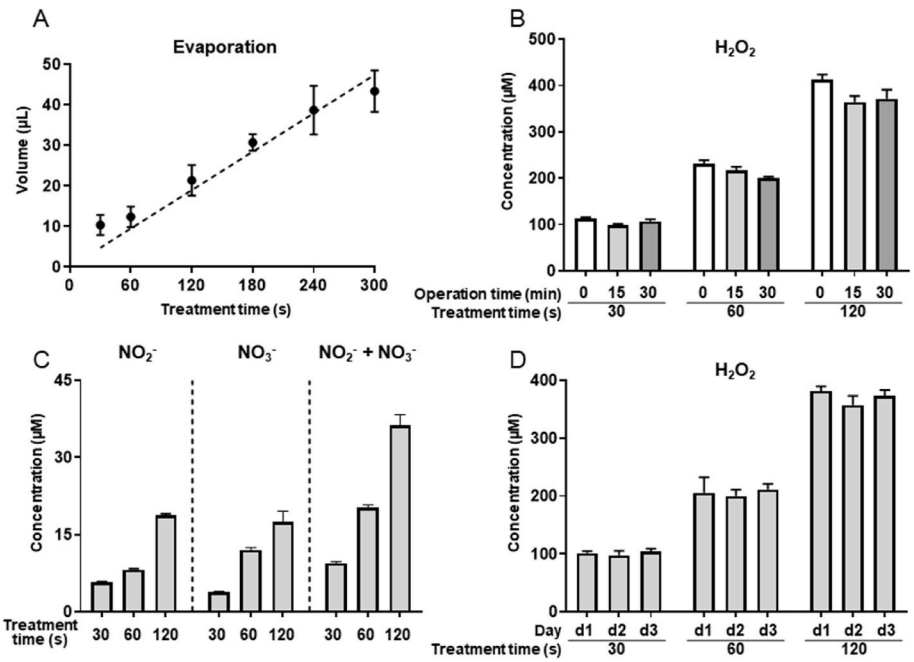

Fig. 2. ROS analyses of plasma-treated liquid. (A) PBS was treated with the plasma in conductive mode for various exposure times, and evaporation was determined. (B) PBS was plasma-treated for 30 s, 60 s, or 120 s immediately after the start (0 min) and after 15 min and 30 min of operation time to measure the concentration of H_2O_2. (C) PBS was plasma-treated for 30 s, 60 s, or 120 s after 15 min of operation time to measure the concentrations of NO_2^- and NO_3^-. (D) To test for the stability of ROS generation, PBS was treated on three consecutive days, and the H_2O_2 concentration was determined. Data are mean + S.D. of one representative experiment with three technical replicates.

also true for the plasma production of nitrite (NO_2^-) and nitrate (NO_3^-) in liquids (Fig. 2C). To test the interassay stability of the plasma ignition in terms of ROS production, we measured H_2O_2 production on three consecutive days and found comparable H_2O_2 levels over time (Fig. 2D). The data suggested the micro plasma jet operation to be stable over time.

3.2. Toxicity of plasma treatment toward different cell lines

Different human cell lines were employed to determine the effect of plasma treatment on cell viability, metabolic activity, and transcription factor activity. Flow cytometry was used to determine cell viability 18 h after exposure to plasma by staining for phosphatidyl-serine exposure (Annexin V) and permeabilized cellular membranes (DAPI) (Fig. 3A). Plasma exposure (grey bars) reduced cellular viability in four cell lines in a treatment time-dependent fashion due to apoptosis (Fig. 3B–E), which was partially or fully abrogated by prior addition of the antioxidant NAC (blue bars), catalase (pink bars), or both (blue-pink striped bars), respectively. As expected, treating cells only with the feed and shielding gas without igniting the plasma did not affect cell viability. Nine seconds of plasma treatment inactivated most JE6.1-TPR (lymphocytic) cells (Fig. 3B). By contrast, 90 s of plasma treatment were required to inactivate most Calu-3 cells (Fig. 3E), an epithelial cell line. The monocytic cell line THP-1-R (Fig. 3C) and the epithelial HaCaT cells (Fig. 3D) were more robust than JE6.1-TPR but not as resistant as Calu-3 cells. To verify the apoptotic nature of cell death while excluding more severe physical stressors which can cause toxicity, we analyzed necrotic cell death by staining for cell membrane rupture in JE6.1-TPR and THP-1-R cells 1 h after plasma treatment. Here, the exposure time was extended more than six-fold (60 s; JE6.1-TPR) or two-fold (120 s; THP-1-R) to the originally longest exposure time (Fig. 3B and C). Notwithstanding, no necrotic action of plasma treatment was observed (Fig. 3F). This does not imply that the 60 s plasma treatment was not toxic but instead suggests that plasma-induced toxicity was not of necrotic but apoptotic nature, as phosphatidylserine exposure takes about 8–10 h post plasma treatment in lymphocytes [25]. Plasma exposure also reduced the metabolic activity in those cells in a treatment time-dependent manner, which also correlated with the cellular survival as expected (Fig. 3G). The data suggested plasma treatment to confer apoptosis but not necrosis in a ROS and cell-type-specific fashion *in vitro*.

3.3. Conductive plasma exposure is potent and modulates transcription factor activity

Plasma jets can be either in contact with their target, usually accompanied by a visual intensification of the plasma effluent (Fig. 4A), or remote to its target (Fig. 4B), where a cloud of ROS diffuses onto the surface. The treatment modality also is of potential clinical relevance [26]. Therefore, conductive and non-conductive plasma treatments were compared side by side. While the longest plasma exposure time in conductive mode nearly completely abolished cell viability in four human cell lines, non-conductive plasma treatment was much less potent (Fig. 4C–F). Cytotoxic effects were evident in JE6.1-TPR and HaCaT cells in non-conductive plasma treatment; these cells were also most sensitive to conductive plasma treatment, and to a lesser extent in THP-1-R cells. Reduction in viability was not observed in Calu-3 cells. Subsequent comparison of H_2O_2 generation revealed five-fold increased production in conductive over non-conductive mode (Fig. 4G), suggesting a significantly decreased introduction of other short-lived ROS between both treatment modalities. Next, we studied whether plasma-derived ROS (conductive mode) affected transcription factor activity. Only live cells were used for this evaluation. In THP-1-R reporter cells, NFκB activity modestly increased with increased plasma treatment times (Fig. 5A), which was abrogated in the presence of the antioxidant NAC (Fig. 5B). By contrast, in JE6.1-TPR cells, the activity of the antioxidant transcription factor AP-1 was not markedly increased with the exception of a plasma exposure time of 3 s (Fig. 5C), which was reduced with prior NAC or catalase addition (Fig. 5D). NFAT activity was strongly increased with plasma exposure (Fig. 5E), which was partially (NAC) or fully (catalase) abrogated by ROS removal (Fig. 5F). NFκB activity in JE6.1-TPR was also slightly increased after plasma treatment (Fig. 5G), although not as pronounced as NFAT activity, and could be inhibited by adding antioxidants (Fig. 5H). Calcium plays an important role in transcription factor activation. Plasma treatment increased intracellular calcium rapidly (Fig. S1A,B). In line, NFAT activation in JE6.1-TPR cells was markedly decreased when scavenging calcium using the calcium chelator BAPTA-AM (Fig. S1C).

The data suggested particularly effective ROS production and transcription factor activation of conductive plasma exposure.

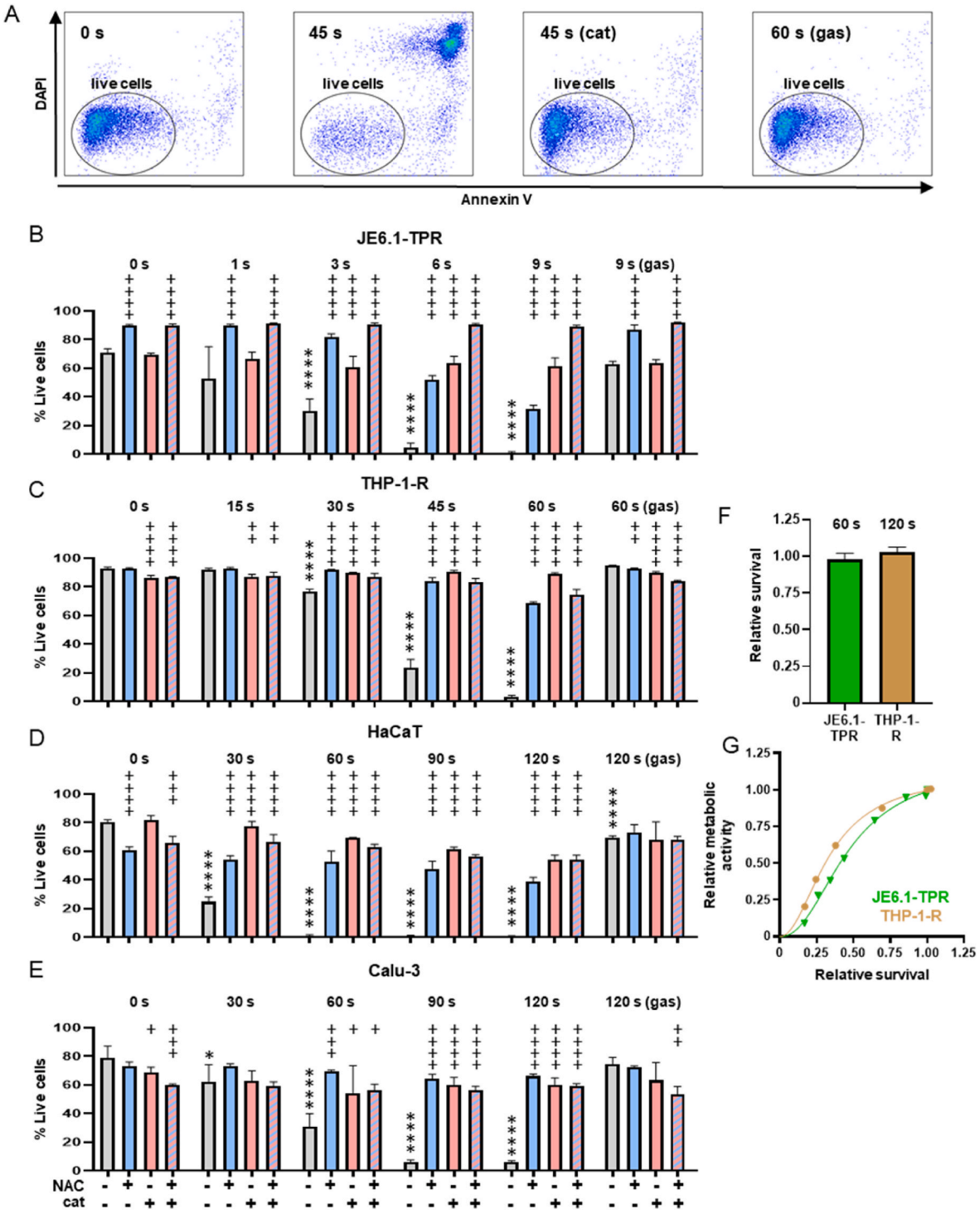

Fig. 3. Toxicity of plasma exposure in four human cell lines. (A) Exemplary gating scheme of live cells after exclusion of cell doublets and debris. Shown are THP-1-R cells untreated (first picture), after 45 s of plasma treatment without (second picture) or with (third picture) catalase (cat), and after 60 s of treatment with non-ignited gases (gas; last picture). (B–E) Two suspension (JE6.1-TPR, B; THP-1-R, C) and two adherent (HaCaT, D; Calu-3, E) cell lines were plasma-treated, and their viability was measured 18 h later by Annexin V and DAPI or Zombie NIR staining and flow cytometry. If indicated, the antioxidant NAC and/or catalase were added immediately before plasma treatment. To measure the influence of the gas stream alone, the cells were also treated with the non-ignited feed and shield gases (gas; plasma = off). (F) No plasma-induced necrosis could be detected in JE6.1-TPR and THP-1-R cells using live/dead-staining 1 h after plasma treatment. Survival is shown relative to untreated control cells. (G) Measurement of the metabolic activity of JE6.1-TPR and THP-1-R cells and its relation to survival (flow cytometry) 18 h after plasma treatment for various times. Both metabolic activity and survival are shown relative to untreated control cells. Data are mean + S.D. of one representative experiment with four technical replicates. Statistical analysis was performed using one-way analysis of variance (ANOVA) ($^{*/+}p<0.05$, $^{**/++}p<0.01$, $^{***/+++}p<0.001$, and $^{****/++++}p<0.0001$. Asterisks indicate a significant difference towards the respective "0 s treatment time"-group; only groups without added antioxidants were compared. Pluses indicate a significant difference towards the "non-antioxidant"-group (grey bars) within the respective treatment time.

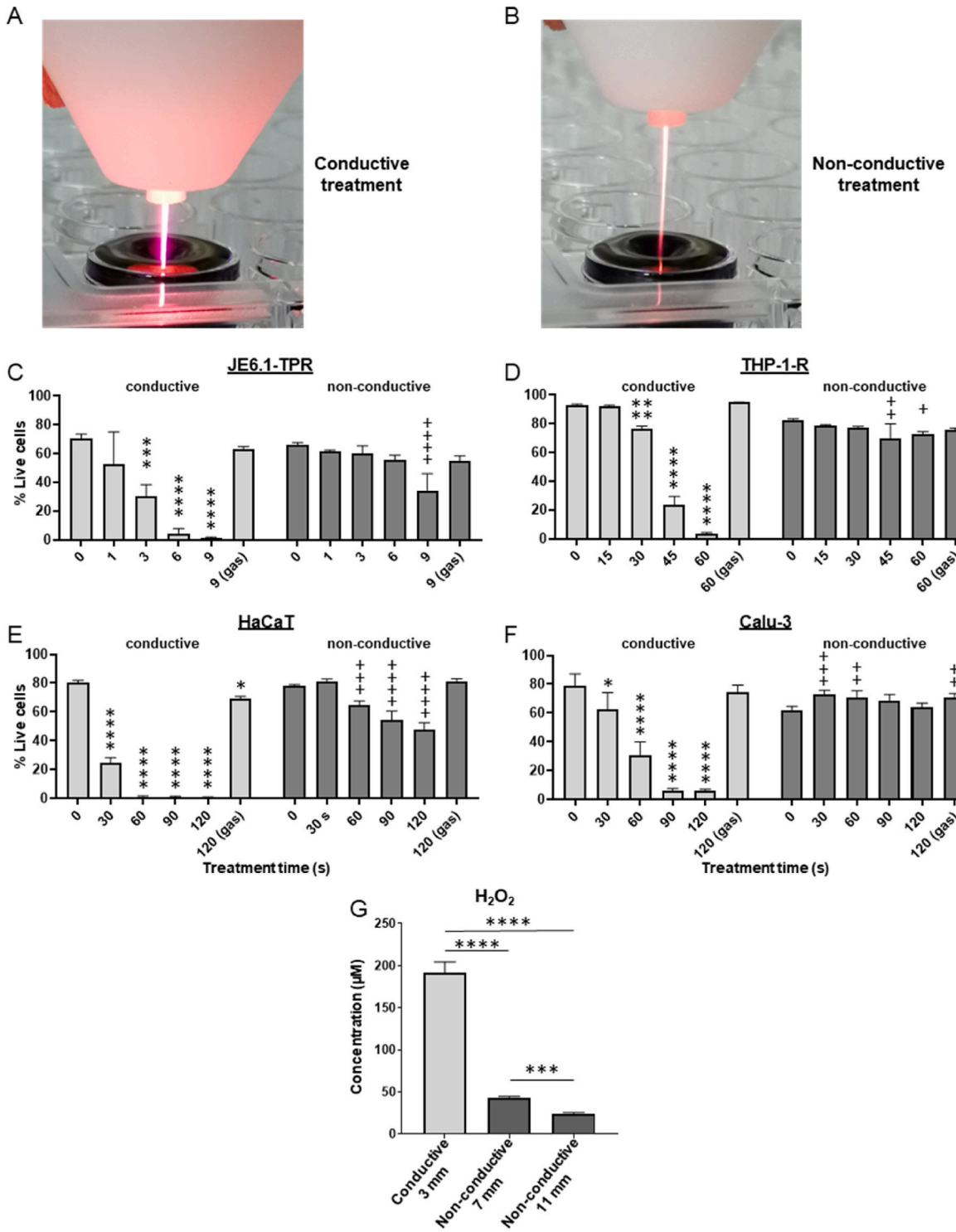

Fig. 4. Conductive and non-conductive plasma exposure comparison. (A, B) Photographs of plasma treatment in conductive (A) or non-conductive (B) mode. For better visualization, PBS was stained with crystal violet, and a larger volume of liquid was used than in the experiments. (C–F) Cells (JE6.1-TPR, C; THP-1-R, D; HaCaT, E; Calu-3, F) were treated either conductively or non-conductively with the micro plasma jet. After 18 h, their viability was assessed by live/dead-staining, followed by flow-cytometric measurements. To measure the influence of the gas stream alone, the cells were also treated with the non-ignited feed and shield gases (gas). (G) The micro plasma jet treatment was employed either in conductive or non-conductive mode for 60 s to determine the mode-dependent differences in H_2O_2 production. Data are mean + S.D. of one representative experiment with three technical. Statistical analysis was performed using one-way analysis of variance (ANOVA) ($^{*/+}p<0.05$, $^{**/++}p<0.01$, $^{***/+++}p<0.001$, $^{****/++++}p<0.0001$). Asterisks indicate a significant difference towards the respective "0 s treatment time"-group for conductively treated cells (C–F). Pluses indicate a significant difference towards the respective "0 s treatment time"-group for non-conductively treated cells (C–F). (For interpretation of the references to colour in this figure legend, the reader is referred to the Web version of this article.)

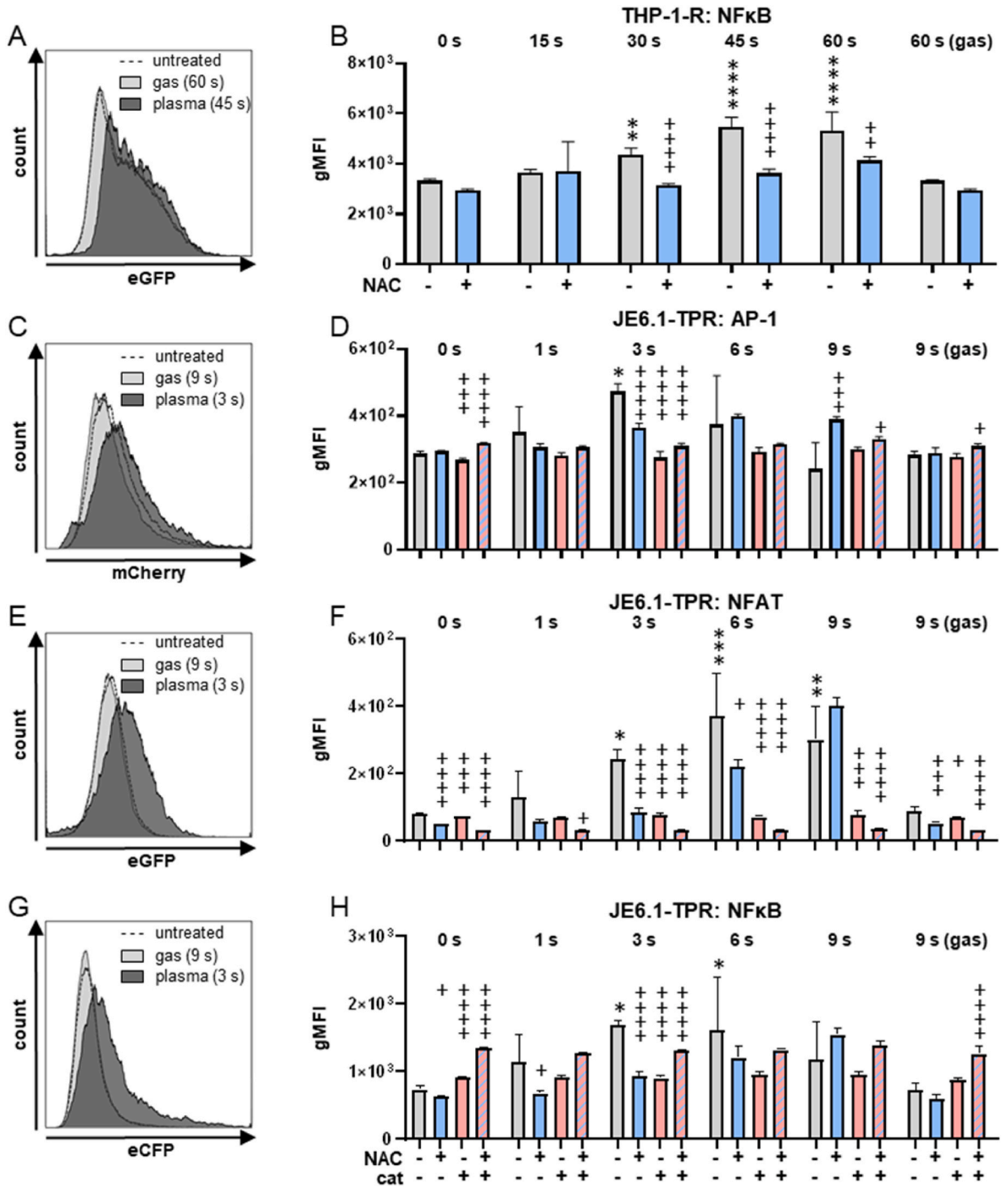

Fig. 5. Influence of plasma exposure on the activity of transcription factors. (A, C, E, G) Representative histograms showing the expression of fluorescent reporter proteins. Untreated cells are shown in dashed lines, gas stream controls in light grey, and plasma-treated cells (45 s for THP-1-R and 3 s for JE6.1-TPR) in dark grey. (B, D, F, H) THP-1-R (B) or JE6.1-TPR (D, F, H) cells were plasma-treated, and transcription factor activity was determined 18 h later by measuring the fluorescent reporter signal via flow cytometry. If indicated, the antioxidant NAC and/or catalase (cat) were added directly before plasma treatment to scavenge ROS. To measure the influence of the gas stream alone, the cells were also treated with the non-ignited feed and shield gases (gas). Data are mean + S.D. of one representative experiment with four technical replicates. Statistical analysis was performed using one-way analysis of variance (ANOVA) ($^{*/+}p<0.05$, $^{**/++}p<0.01$, $^{***/+++}p<0.001$, $^{****/++++}p<0.0001$). Asterisks indicate a significant difference towards the respective "0 s treatment time"-group; only groups without added antioxidants were tested. Pluses indicate a significant difference towards the "non-antioxidant"-group (grey bars) within the respective treatment time.

3.4. Antiviral plasma activity against murine coronaviruses

We measured the effect of plasma exposure on the inactivation of viruses by determining the viral titer of treated viral suspensions via plaque assay and by observing the inhibition of host cell metabolism after infection with plasma-treated viruses (Fig. 6). A 5 min plasma treatment reduced the virus titer (Fig. 7A) by a factor of about 10 (Fig. 7B). By adding NAC alone or in combination with catalase (cat), abrogation of antiviral effects was only minimal, while catalase addition alone showed no effect (Fig. 7B). This was surprising as both agents protected cells from toxic plasma effects, while the plasma treatment time-dependent reduction of viral infectivity was more in line with

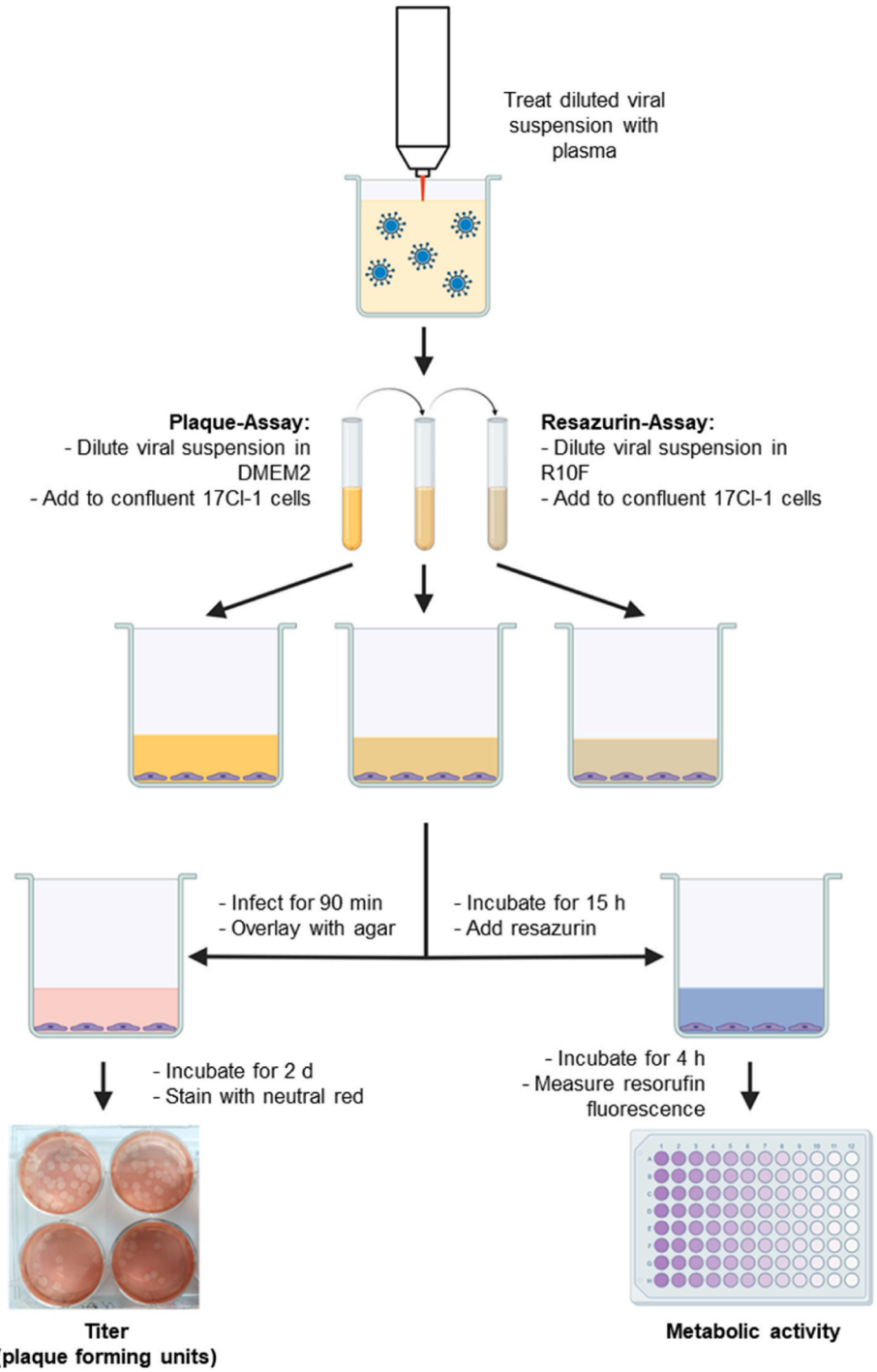

Fig. 6. Experimental setup for MHV experiments. MHV was plasma-treated, and virus suspensions were used either in a plaque assay to determine viral titer or to infect host cells to study infection-induced changes in metabolic activity.

results observed with human cell lines (Fig. 7C). Above 7.5 min of plasma treatment, all viruses in the solution were inactivated according to the plaque formation experiments. Interestingly, the addition of NAC and catalase prior to such long plasma treatment times showed little but evident protection of the virus' cytolytic activity. Nevertheless, this protective effect declined over time, most likely explained by the inactivation of those agents after prolonged plasma treatment time. For instance, catalase abrogated H_2O_2 deposition in liquids up to 3 min of conductive treatment, while a pronounced accumulation of H_2O_2 could be observed at 5 min exposure (Fig. S2). Investigating the antiviral activity of non-conductive plasma exposure, it was found that its potency in reducing cytolytic viral activity was markedly impaired by a factor of seven (Fig. 7D), which corroborates results on cytotoxic plasma effects achieved in human cell lines. To verify the results on antiviral plasma activity using another method, we infected 17Cl-1 cells with virus suspensions and measured the cells' metabolic activity 15 h later by analyzing their capability of resazurin reduction (Fig. 7E). At high virus concentrations (1:10 dilution of virus suspension), already reduced metabolic activities were slightly enhanced by plasma treatment. At low virus concentrations (1:10,000), there were barely any differences in metabolic activities observed compared to uninfected cells. However, at intermediate virus concentrations (dilutions of 1:100 or 1:1000), more

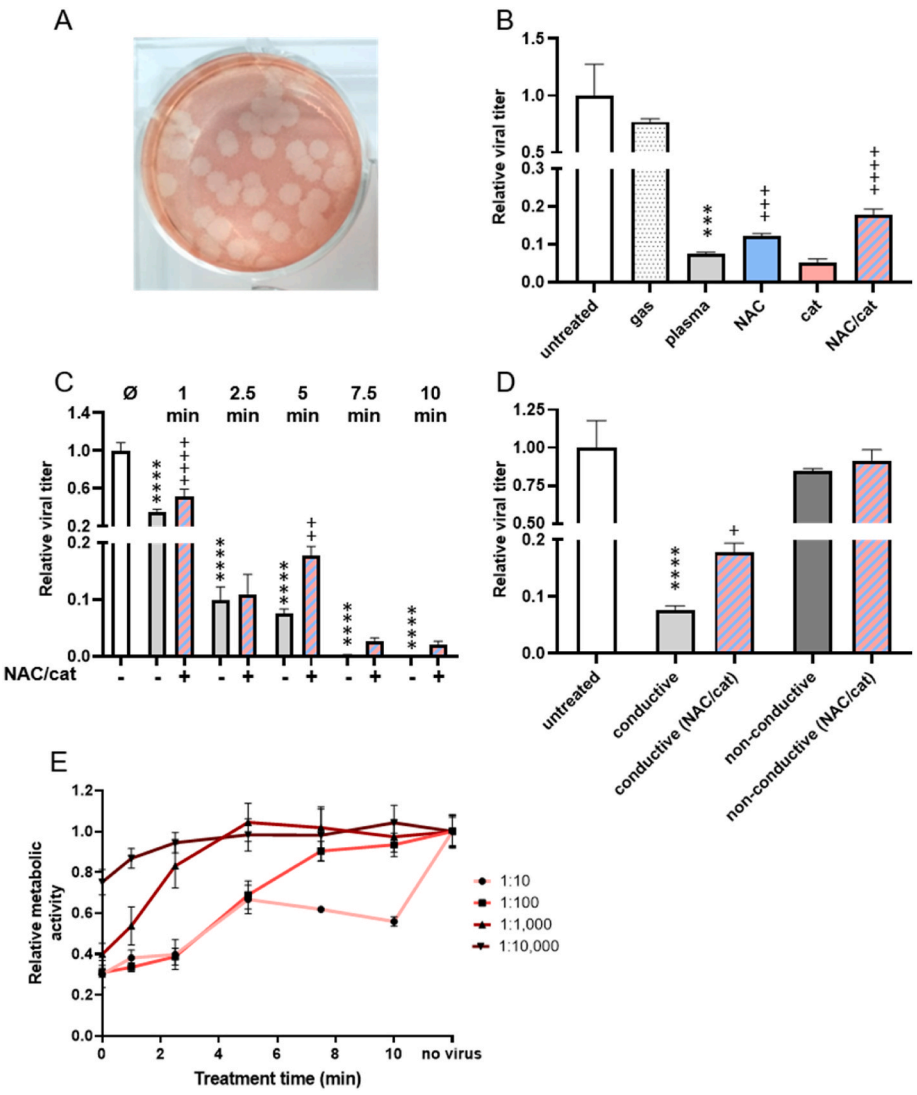

Fig. 7. Plasma exposure of MHV-containing liquids was antiviral. (A) Representative result of a plaque assay after neutral red-staining. (B, C) Viral suspensions were plasma-treated (plasma, 5 min) with or without NAC and/or catalase (cat) before viral titers were determined using the plaque assay and set in relation to the untreated MHV control (B), and dose-response relations after different durations of plasma treatment (C). To measure the influence of the gas stream alone (B), the viruses were also treated with the non-ignited feed and shield gases (gas). (D) Relative titers of viral suspensions that were plasma-treated for 5 min either conductively or non-conductively in the presence or absence of NAC and/or catalase (cat). (E) Viral suspensions were plasma-treated for different exposure times, diluted, and used to infect 17Cl-1 cells. 15 h later, the metabolic activity was measured by resazurin reduction and compared to untreated cells. Data are mean + S.D. of one representative experiment with at least three technical replicates. Statistical analysis was performed using one-way analysis of variance (ANOVA) ($^{*/+}p<0.05$, $^{**/++}p<0.01$, $^{***/+++}p<0.001$, $^{****/++++}p<0.0001$). Asterisks indicate a significant difference towards untreated viral suspensions; only groups without added antioxidants were tested. Pluses indicate a significant difference towards the respective plasma-treated viral suspensions containing no antioxidants. (For interpretation of the references to colour in this figure legend, the reader is referred to the Web version of this article.)

extended plasma treatment (beyond 4 min) enhanced metabolic activities of infected cells to levels comparable to non-infected ones suggesting plasma-mediated reduction of viral loads. The data indicate a potent antiviral plasma activity in the conductive mode against a murine coronavirus model infection *in vitro*.

Conductivity amplifies in particular the local generation of short-lived species. The marked differences in antiviral activity in non-conductive and conductive mode, in line with the diminished rescue effects of H_2O_2 degrading catalase, pointed to an increased importance of short-lived species concerning the virucidal activity of plasma. To further elucidate the mode of action, deposition of singlet oxygen ($^1O_2$), peroxynitrite ($ONOO^-$), hydroxyl radicals ($^{\cdot}OH$), and hypochlorous acid (HOCl) was assessed in PBS and R2F using redox-sensitive probes, with reduced levels detected in the latter. Unsurprisingly, neither addition of catalase or H_2O_2 influenced levels of short-lived ROS in the liquids (Fig. 8A–C). Next, different substances were tested for their scavenging ability regarding the respective species. Hereof, trolox and ascorbic acid proved to be highly efficient scavengers of short-lived ROS/RNS (Fig. 8D–F) and were chosen for further protection assays with MHV. As MHV plasma treatment took place with viruses being suspended within a liquid, we also considered plasma-induced changes in liquid temperature as a potential factor in the mechanism of action. Surprisingly, during the course of plasma treatment, the temperature did not increase but rather decreased within the bulk liquid (Fig. 8G). This, however, does not rule out micro-increases of the temperature at the small spots where the plasma streamers contact the liquid, which could have led to a short (microseconds) and local (several dozens to hundreds of micrometers) temperature rise that may have contributed to the effects observed. However, we did not have the technical setup to generate temperature maps of liquid surfaces at high spatio-temporal resolutions. With regard to the antioxidants and potential protection from plasma-mediated inactivation, interestingly, a virucidal effect was already observed after addition of ascorbic acid alone, while a rescue effect after plasma treatment could not be observed for this vitamin C agent (Fig. 9A and B). By contrast, a significant rescue effect could be observed with trolox. Synergistic effects with catalase could not be observed, again pointing to the impact of short-lived species (Fig. 9C and D). In both cases, the results of the plaque assay were mirrored by the metabolic activity of infected cells, providing evidence of the validity of this method (Fig. 9B,D).

4. Discussion

During the SARS-CoV-2 pandemic, it became increasingly clear that societies need novel ways of passive and active control of virus infection. Plasma technology may be suitable for superficial virus inactivation [17]. Employing an optimized micro plasma jet with the potential to directly reach small nasopharyngeal cavities, we investigated the

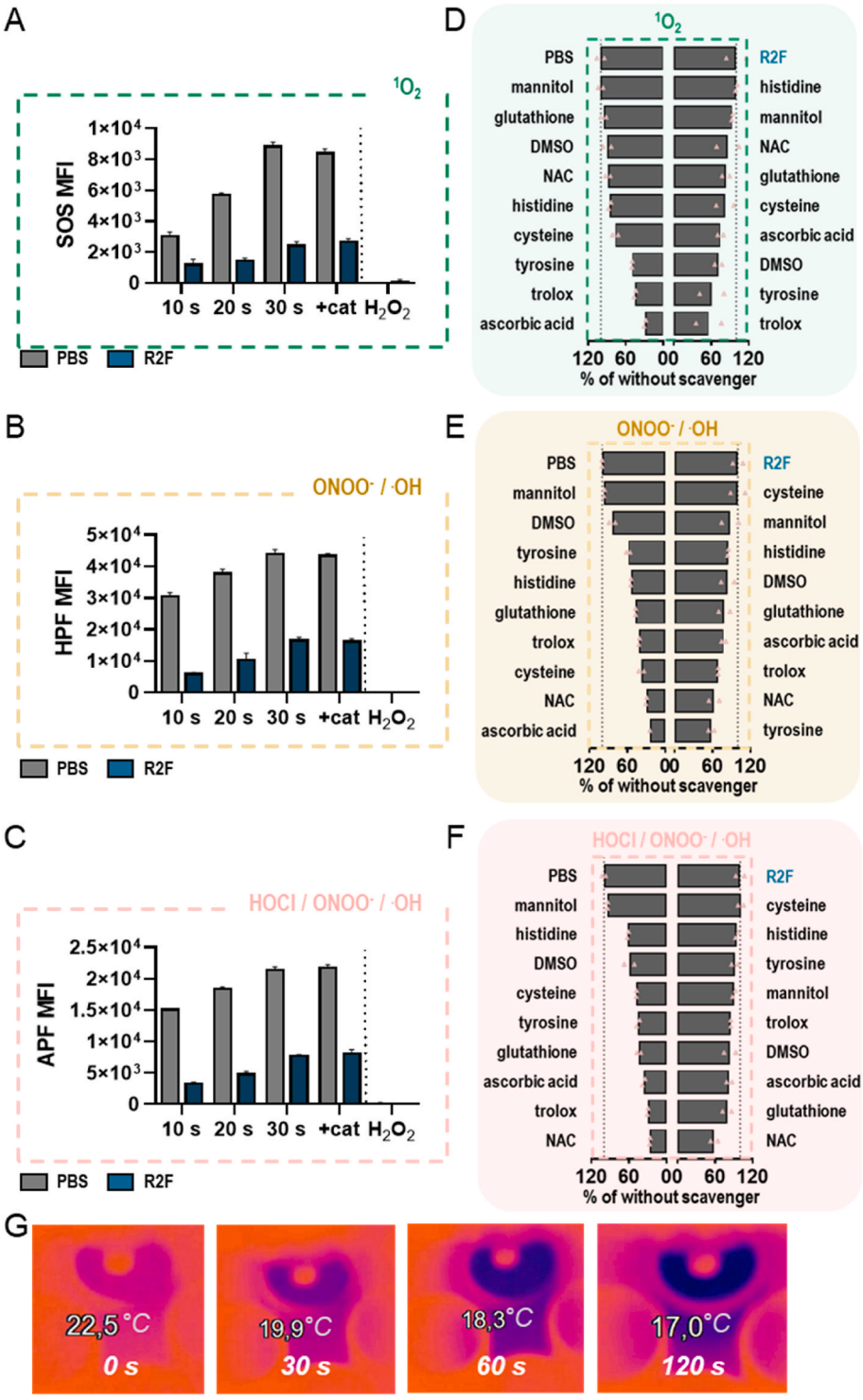

Fig. 8. Screening of different ROS scavengers and temperature. (A–C) Mean fluorescence intensities (MFI) of singlet oxygen sensor (SOS) indicative of singlet oxygen ($^1O_2$; A), hydroxyphenyl fluorescein (HPF) indicative of peroxynitrite ($ONOO^-$) and hydroxyl radicals ($^·OH$; B) and aminophenyl fluorescein (APF) indicative of $ONOO^-$, $^·OH$, and hypochlorous acid (HOCl, C) after plasma treatment of PBS or R2F for 10 s, 20 s, 30 s, 30 s + catalase (+Cat), or experimentally addition of 50 μM hydrogen peroxide without plasma treatment (H_2O_2). (D–F) Screening of different molecules for their scavenging activity during 30 s plasma treatment of PBS and R2F using ROS sensitive probes indicative of $^1O_2^-$ (SOS; D), $ONOO^-$ and $^·OH$ (HPF; E) or $ONOO^-$, $^·OH$, and HOCl (APF; F). (G) Temperature of PBS before (left) and during (middle to right) plasma treatment, showing a decrease rather than increase of temperature. Bar graphs show mean ± standard error of the mean (SEM; A-C) or individual values (D–F) of one to two experiments.

plasma source's cytotoxicity and antiviral activity using a murine coronavirus *in vitro* infection model.

Plasma exposure showed powerful effects in reducing viral loads and infectivity in the MHV model *in vitro*. This is in line with other studies investigating the antiviral effectivity of different types of plasma sources, albeit the effect size strongly depends on the specific virus model and plasma source types employed [8]. Several log-reduction were observed, for instance, when tested on MS2 phages [27], Tulane virus [28], human herpes simplex virus type 1 [29], feline calicivirus [30], and respiratory syndrome virus [31]. Many of the studies performed to analyze antiviral cold plasma effects are aimed at virus removal from inanimate matrices or surfaces, such as food, packaging, air, and liquids [8]. However, studies investigating the plasma's antiviral activity in clinically relevant model systems, such as infected animals, are not available yet. Also the present study is limited to the analysis of antiviral effects in a plasma-treated liquid, which is stirred by convection forces introduced through the plasma jet's feed gas flow that, through mixing, enables interactions between plasma-generated antiviral compounds and viral particles [32]. By contrast, the depth by which plasma-generated compounds can penetrate into virus-infected tissues

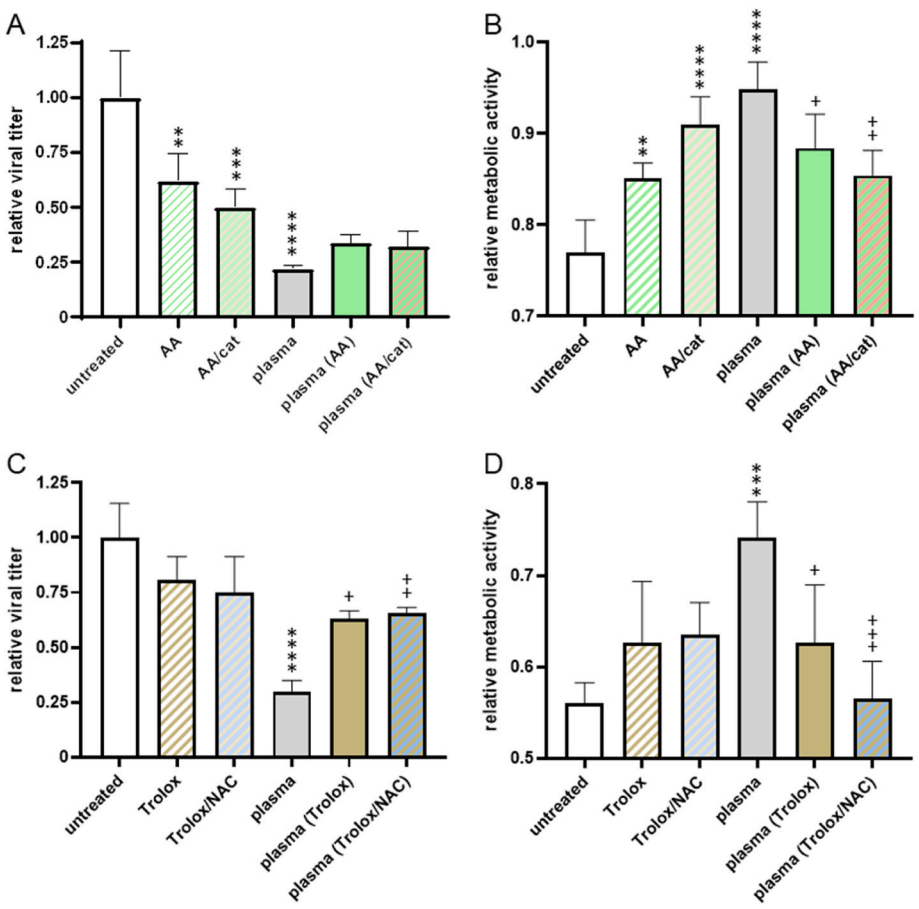

Fig. 9. Short-lived plasma-derived ROS were antiviral. (A) Viral suspensions were incubated with ascorbic acid alone or in combination with catalase (cat) for 15 min or mixed with these agents and treated with plasma for 1 min. Afterward, viral titers were determined using the plaque assay and set in relation to the untreated MHV control conditions. (B) Viral suspensions were treated as in (A), diluted 1:2,500, and used to infect 17Cl-1 cells. 15 h later, the metabolic activity was measured by resazurin reduction and compared to untreated cells. (C) Viral suspensions were incubated with trolox alone or in combination with NAC for 15 min or mixed with these agents and treated with plasma for 1 min. Afterward, viral titers were determined using the plaque assay and set in relation to the untreated MHV control. (D) Viral suspensions were treated as in (C), diluted 1:2,500, and used to infect 17Cl-1 cells. 15 h later, the metabolic activity was measured by resazurin reduction and compared to untreated cells. Data are mean + S.D. of one representative experiment with three to four technical replicates. Statistical analysis was performed using one-way analysis of variance (ANOVA) ($^{*/+}p<0.05$, $^{**/++}p<0.01$, $^{***/+++}p<0.001$, $^{****/++++}p<0.0001$). Asterisks indicate a significant difference towards untreated viral suspensions. Pluses indicate a significant difference towards the respective plasma-treated viral suspensions containing no antioxidants.

might be more limited, at least as plasma depth cytotoxicity studies in relevant model systems suggest [33]. A recent study indicated decreased SARS-CoV-2 uptake via downregulation of its entry port, the ACE2 receptor [34], upon exposure to long-lived species present in plasma-treated liquids [35].

Several modes of action may be held accountable for the antiviral plasma effects observed. The murine hepatitis virus is an enveloped RNA virus of an average size of 86 nm [36]. Most likely, plasma-derived ROS damaged the lipid membrane. Different mechanisms have been suggested in this process. One relates to the formation of ROS-derived pores via head group and lipid tail oxidation, introduced via hydroxyl radicals, for instance Ref. [37]. Consequently, more ROS might have entered the viral particle to render its cargo dysfunctional. Alternatively or in parallel, lipid peroxidation has been described in cold plasma-treated cells [38], a process known to reduce viral infectivity via impairment of lipid envelopes and protein shells [39]. Another, more subtle mechanism relates to oxidative post-translational modifications (oxPTMs) of viral proteins, such as the M-protein of MHV. We have recently described the diverse landscapes of such plasma-derived oxidative modifications in amino acids [40], peptides [41], proteins [42], and lipids [43]. Functional changes were also observed for proteins and enzymes, pointing to practical consequences of such modifications, such as reduced effectivity of viral entry into cells. Recently, using influenza viruses, lipid peroxidation was demonstrated to reduce viral transmission and infectivity [44], underlining the putative role of ROS in explaining our results.

However, a surprising result was the limited capability of the ROS scavenger NAC and the H_2O_2-degrading catalase to protect MHV from plasma-induced damage. This was even more unexpected as both substances did protect plasma-treated cells from plasma-mediated cytotoxic effects. However, H_2O_2 is a primary inducer of cytotoxicity in eukaryotic cells [45], which can be abrogated by catalase [46]. At the same time, H_2O_2 is generally considered a weak oxidant [47]. It might not damage viral particles to a greater degree at relatively low concentrations. Human cell lines but not virus particles were protected from plasma treatment by adding catalase. Therefore, the plasma-mediated inactivation of catalase seems a less likely explanation for understanding catalase's inability to protect viral particles. It is more likely that an H_2O_2-independent mechanism was involved in plasma-mediated inactivation of virus particles. Strikingly, notable rescue effects were achieved by addition of trolox, pointing to the importance of short-lived species in the virucidal effects of plasma. In line, ozone and its precursor atomic oxygen as well as singlet delta oxygen generated by plasmas [48], have been described as antiviral agents before [39,49]. One possible explanation for the lower ability of anti-ROS agents to protect larger objects, such as cells, better from plasma-mediated effects than smaller objects, such as viruses, is the relative likelihood of smaller objects entering the plasma-liquid interphase. This may happen because of their smaller size, allowing complete penetration into the interphase, and their higher number [48]. In the interphase, diffusion distances of the plasma gas phase-derived species to target objects such as viruses are minimal, reducing the likelihood of antioxidants to protect such objects by inactivating reactive species. This could also be the reason why stronger effects were seen for the conductive over non-conductive mode because, in the conductive mode, ROS transport from the plasma jet to the liquid is maximized [50,51]. A temperature increase in conductive mode has been described before [26] and might contribute to ROS-independent effects. However, as indicated by infrared spectroscopy measurements, temperature differences could not be observed for the micro plasma jet used in the present study (data now shown). Moreover, we cannot exclude non-ROS-related effects, e.g., UV radiation, electric fields and changes in pH, that have been described as contributors to virus inactivation before [8], albeit only secondary to

ROS/RNS. It has become a standard in the field of plasma technology research to test the cytotoxicity of novel plasma sources, which we had implanted using four different cell lines (JE6.1-TPR, THP-1-R, Calu-3, and HaCaT). Sensitivity to plasma treatment varied considerably among the different cell lines, with JE6.1-TPR being the most sensitive and Calu-3 the most robust one. What determines the sensitivity of a cell towards plasma treatment is still unknown. However, there are hypotheses linking either the expression of aquaporins [52], the expression of redox-related enzymes [53], the cholesterol content of the cell membrane [54,55], or the baseline metabolic rate of the cell [56]. We cannot draw any conclusions on this point from our data, but the results of this study are consistent with the results of one of our previous studies that were performed with the atmospheric pressure argon plasma jet kINPen [56]. Jurkat cells were more sensitive than HaCaT and THP-1 cells in both studies. Considering that JE6.1-TPR are modified Jurkat cells, it is very likely that the points discussed also apply to JE6.1-TPR.

Our data indicate the induction of programmed cell death upon plasma treatment rather than necrotic cell death. This is in line with other publications [57,58]. The inhibition of cell death by adding NAC and/or catalase shows that ROS are the main effectors. However, it is worth noting that NAC failed to fully protect JE6.1-TPR cells after short (9 s) plasma treatment, whereas it does this for a longer (120 s) treatment time of Calu-3 cells. Therefore, it is unlikely that the antioxidative capacity of NAC is exhausted after only a few seconds. There are either other ROS not scavenged by NAC that affect the viability of individual cell lines or ROS-independent mechanisms influence the viability. For example, cell death following plasma treatment has been associated earlier with electromagnetic fields, charged particles, and UV radiation [59,60].

Transcription factors are essential for regulating cellular processes such as cell cycle progression, activation, proliferation, and cell death [61,62]. ROS can influence the expression and activation of transcription factors like AP-1 [63,64], NFAT [65,66], and NFκB [63,64,67] and thereby the general constitution and fate of the cell. As plasma generates large amounts of ROS, effects on transcription factors are evident, as our data suggest. For example, NFAT transcription factors regulate apoptosis, with NFAT1 being a pro-apoptotic member of this family [68–70]. Therefore, its activity in JE6.1-TPR cells could be a part of programmed cell death induced by plasma treatment. Furthermore, von Knethen et al. found in the RAW264.7 macrophage-like cell line that AP-1 and NFκB activation by nitric oxide, as commonly produced by cold plasmas [71], can attenuate apoptotic cell death by promoting cyclooxygenase-2 (Cox-2) expression [72]. It is therefore conceivable that the activation of specific transcription factors is not only a consequence of the induction of programmed cell death, but also a means for the cells to prevent this through a change in transcription factor activity triggered by ROS stress.

5. Conclusion

We have investigated an optimized neon-driven micro plasma jet and determined its potent ROS production and *in vitro* antiviral activity in a murine coronavirus infection model. As expected, the cytotoxic effects of the atmospheric pressure plasma jet in eukaryotic cells depended mainly on the cell line's source. All effects were maximal when the plasma was in direct contact with its liquid target (conductive mode) and were abrogated to a large and small extent in non-conductively plasma-treated cells and virus suspensions, respectively. Future studies on primary cells from human sources and on the plasma's tissue surface antiviral activity and the key antiviral ROS are needed to determine the relevance for practice and mechanisms of our findings.

Funding

Funding was received from the German Federal Ministry of Education and Research (BMBF, grant numbers 03COV06A, 03COV06C, 03Z22DN11, and 03Z22Di1).

Declaration of competing interest

The authors have no conflict of interest to declare.

Data availability

Data will be made available on request.

Acknowledgments

We would like to thank Volker Thiel, Nadine Ebert, and Lisa Thomann (all Vetsuisse Faculty, University Bern, Switzerland) for providing 17Cl-1 cells and MHV-A59 reporter viruses; and Peter Steinberger and Claire Battin (both Medical University of Vienna, Austria) for providing JE6.1-TPR and THP-1-R cells. Technical support by Felix Niessner is gratefully acknowledged.

Appendix A. Supplementary data

Supplementary data related to this article can be found at https://doi.org/10.1016/j.freeradbiomed.2022.08.026.

References

[1] M. Palacios Cruz, et al., Covid-19, a worldwide public health emergency, Rev. Clin. Esp. 221 (2021) 55–61, https://doi.org/10.1016/j.rceng.2020.03.001.
[2] R. Sommerstein, et al., Risk of sars-cov-2 transmission by aerosols, the rational use of masks, and protection of healthcare workers from covid-19, Antimicrob. Resist. Infect. Control 9 (2020) 100, https://doi.org/10.1186/s13756-020-00763-0.
[3] M. Alimohammadi, et al., Effectiveness of ozone gas on airborne virus inactivation in enclosed spaces: a review study, Ozone: Sci. Eng. 43 (2020) 21–31, https://doi.org/10.1080/01919512.2020.1822149.
[4] J. Hadi, et al., Control measures for sars-cov-2: a review on light-based inactivation of single-stranded rna viruses, Pathogens 9 (2020), https://doi.org/10.3390/pathogens9090737.
[5] A.M. Elsaid, et al., A critical review of heating, ventilation, and air conditioning (hvac) systems within the context of a global sars-cov-2 epidemic, Process Saf. Environ. Protect. 155 (2021) 230–261, https://doi.org/10.1016/j.psep.2021.09.021.
[6] I. Assadi, et al., Review on inactivation of airborne viruses using non-thermal plasma technologies: from ms2 to coronavirus, Environ. Sci. Pollut. Res. Int. 29 (2022) 4880–4892, https://doi.org/10.1007/s11356-021-17486-3.
[7] A. Filipic, et al., Cold plasma, a new hope in the field of virus inactivation, Trends Biotechnol. 38 (2020) 1278–1291, https://doi.org/10.1016/j.tibtech.2020.04.003.
[8] H. Mohamed, et al., Non-thermal plasma as a novel strategy for treating or preventing viral infection and associated disease, Front. Phys. 9 (2021), https://doi.org/10.3389/fphy.2021.683118.
[9] M. Weiss, et al., Virucide properties of cold atmospheric plasma for future clinical applications, J. Med. Virol. 89 (2017) 952–959, https://doi.org/10.1002/jmv.24701.
[10] A. Privat-Maldonado, et al., Ros from physical plasmas: redox chemistry for biomedical therapy, Oxid. Med. Cell. Longev. 2019 (2019), 9062098, https://doi.org/10.1155/2019/9062098.
[11] I. Adamovich, et al., The 2017 plasma roadmap: low temperature plasma science and technology, J. Phys. D Appl. Phys. 50 (2017), 323001, https://doi.org/10.1088/1361-6463/aa76f5.
[12] S. Barroug, et al., Combination of natural compounds with novel non-thermal technologies for poultry products: a review, Front. Nutr. 8 (2021), 628723, https://doi.org/10.3389/fnut.2021.628723.
[13] C. Hertwig, et al., Cold atmospheric pressure plasma and low energy electron beam as alternative nonthermal decontamination technologies for dry food surfaces: a review, Trends Food Sci. Technol. 77 (2018) 131–142, https://doi.org/10.1016/j.tifs.2018.05.011.
[14] S. Bekeschus, et al., Medical gas plasma-stimulated wound healing: evidence and mechanisms, Redox Biol. 46 (2021), 102116, https://doi.org/10.1016/j.redox.2021.102116.
[15] P. Bourke, et al., Microbiological interactions with cold plasma, J. Appl. Microbiol. 123 (2017) 308–324, https://doi.org/10.1111/jam.13429.
[16] V. Scholtz, et al., Non-thermal plasma treatment of eskape pathogens: a review, Front. Microbiol. 12 (2021), 737635, https://doi.org/10.3389/fmicb.2021.737635.
[17] S. Bekeschus, et al., Gas plasma technology-an asset to healthcare during viral pandemics such as the covid-19 crisis? IEEE Trans. Radiat. Plasma. Med. Sci. 4 (2020) 391–399, https://doi.org/10.1109/TRPMS.2020.3002658.
[18] J. Winter, et al., On the development of a deployable cold plasma endoscope, Contrib. Plasma Phys. 58 (2018) 404–414, https://doi.org/10.1002/ctpp.201700127.

[19] J. Winter, et al., Enhanced atmospheric pressure plasma jet setup for endoscopic applications, J. Phys. D Appl. Phys. 52 (2019), https://doi.org/10.1088/1361-6463/aae817.

[20] L. Miebach, et al., Tumor cytotoxicity and immunogenicity of a novel v-jet neon plasma source compared to the kinpen, Sci. Rep. 11 (2021) 136, https://doi.org/10.1038/s41598-020-80512-w.

[21] S. Jutz, et al., Assessment of costimulation and coinhibition in a triple parameter t cell reporter line: simultaneous measurement of nf-kappab, nfat and ap-1, J. Immunol. Methods 430 (2016) 10–20, https://doi.org/10.1016/j.jim.2016.01.007.

[22] C. Battin, et al., A human monocytic nf-kappab fluorescent reporter cell line for detection of microbial contaminants in biological samples, PLoS One 12 (2017), e0178220, https://doi.org/10.1371/journal.pone.0178220.

[23] J. Leibowitz, et al., Coronaviruses: propagation, quantification, storage, and construction of recombinant mouse hepatitis virus, Curr. Protoc. Microbiol. (2011), https://doi.org/10.1002/9780471729259.mc15e01s21 (Chapter 15), Unit 15E 11.

[24] J. Winter, et al., Feed gas humidity: a vital parameter affecting a cold atmospheric-pressure plasma jet and plasma-treated human skin cells, J. Phys. D Appl. Phys. 46 (2013), 295401, https://doi.org/10.1088/0022-3727/46/29/295401.

[25] S. Bekeschus, et al., Cold physical plasma treatment alters redox balance in human immune cells, Plasma Med. 3 (2013) 267–278, https://doi.org/10.1615/PlasmaMed.2014011972.

[26] L. Miebach, et al., Conductivity augments ros and rns delivery and tumor toxicity of an argon plasma jet, Free Radic. Biol. Med. 180 (2022) 210–219, https://doi.org/10.1016/j.freeradbiomed.2022.01.014.

[27] T. Xia, et al., Inactivation of airborne viruses using a packed bed non-thermal plasma reactor, J. Phys. D Appl. Phys. 52 (2019), 255201, https://doi.org/10.1088/1361-6463/ab1466.

[28] S.H. Roh, et al., Inactivation of escherichia coli o157:H7, salmonella, listeria monocytogenes, and tulane virus in processed chicken breast via atmospheric in-package cold plasma treatment, LWT (Lebensm.-Wiss. & Technol.) 127 (2020), https://doi.org/10.1016/j.lwt.2020.109429.

[29] O. Bunz, et al., Cold atmospheric plasma as antiviral therapy - effect on human herpes simplex virus type 1, J. Gen. Virol. 101 (2020) 208–215, https://doi.org/10.1099/jgv.0.001382.

[30] G. Nayak, et al., Reactive species responsible for the inactivation of feline calicivirus by a two-dimensional array of integrated coaxial microhollow dielectric barrier discharges in air, Plasma Process. Polym. 15 (2018), https://doi.org/10.1002/ppap.201700119.

[31] G. Nayak, et al., Rapid inactivation of airborne porcine reproductive and respiratory syndrome virus using an atmospheric pressure air plasma, Plasma Process. Polym. 17 (2020), https://doi.org/10.1002/ppap.201900269.

[32] J. Vorac, et al., Gas mixing enhanced by power modulations in atmospheric pressure microwave plasma jet, Plasma Sources Sci. Technol. 25 (2016), https://doi.org/10.1088/0963-0252/25/2/025018.

[33] L.I. Partecke, et al., Tissue tolerable plasma (ttp) induces apoptosis in pancreatic cancer cells in vitro and in vivo, BMC Cancer 12 (2012), https://doi.org/10.1186/1471-2407-12-473.

[34] L. Samavati, et al., Ace2, much more than just a receptor for sars-cov-2, Front. Cell. Infect. Microbiol. 10 (2020) 317, https://doi.org/10.3389/fcimb.2020.00317.

[35] P. Wang, et al., Cold atmospheric plasma for preventing infection of viruses that use ace2 for entry, Theranostics 12 (2022) 2811–2832, https://doi.org/10.7150/thno.70098.

[36] M. Barcena, et al., Cryo-electron tomography of mouse hepatitis virus: insights into the structure of the coronavirion, Proc. Natl. Acad. Sci. U.S.A. 106 (2009) 582–587, https://doi.org/10.1073/pnas.0805270106.

[37] M. Yusupov, et al., Effect of head group and lipid tail oxidation in the cell membrane revealed through integrated simulations and experiments, Sci. Rep. 7 (2017) 5761, https://doi.org/10.1038/s41598-017-06412-8.

[38] J. Van Loenhout, et al., Auranofin and cold atmospheric plasma synergize to trigger distinct cell death mechanisms and immunogenic responses in glioblastoma, Cells 10 (2021), https://doi.org/10.3390/cells10112936.

[39] B.K. Murray, et al., Virion disruption by ozone-mediated reactive oxygen species, J. Virol. Methods 153 (2008) 74–77, https://doi.org/10.1016/j.jviromet.2008.06.004.

[40] J.W. Lackmann, et al., Chemical fingerprints of cold physical plasmas - an experimental and computational study using cysteine as tracer compound, Sci. Rep. 8 (2018) 7736, https://doi.org/10.1038/s41598-018-25937-0.

[41] S. Wenske, et al., Nonenzymatic post-translational modifications in peptides by cold plasma-derived reactive oxygen and nitrogen species, Biointerphases 15 (2020), 061008, https://doi.org/10.1116/6.0000529.

[42] R. Clemen, et al., Gas plasma technology augments ovalbumin immunogenicity and ot-ii t cell activation conferring tumor protection in mice, Adv. Sci. 8 (2021), 2003395, https://doi.org/10.1002/advs.202003395.

[43] J. Striesow, et al., Oxidative modification of skin lipids by cold atmospheric plasma (cap): a standardizable approach using rp-lc/ms(2) and di-esi/ms(2), Chem. Phys. Lipids 226 (2020), 104786, https://doi.org/10.1016/j.chemphyslip.2019.104786.

[44] T. Qin, et al., Catalytic inactivation of influenza virus by iron oxide nanozyme, Theranostics 9 (2019) 6920–6935, https://doi.org/10.7150/thno.35826.

[45] L. Miebach, et al., Gas plasma–oxidized sodium chloride acts via hydrogen peroxide in a model of peritoneal carcinomatosis, Proc. Natl. Acad. Sci. USA 119 (2022), https://doi.org/10.1073/pnas.2200708119.

[46] J. Winter, et al., Tracking plasma generated h2o2 from gas into liquid phase and revealing its dominant impact on human skin cells, J. Phys. D Appl. Phys. 47 (2014), 285401, https://doi.org/10.1088/0022-3727/47/28/285401.

[47] H. Sies, et al., Defining roles of specific reactive oxygen species (ros) in cell biology and physiology, Nat. Rev. Mol. Cell Biol. (2022), https://doi.org/10.1038/s41580-022-00456-z.

[48] P.J. Bruggeman, et al., Plasma-liquid interactions: a review and roadmap, Plasma Sources Sci. Technol. 25 (2016), 053002, https://doi.org/10.1088/0963-0252/25/5/053002.

[49] D. Korneev, et al., Ultrastructural aspects of photodynamic inactivation of highly pathogenic avian h5n8 influenza virus, Viruses 11 (2019), https://doi.org/10.3390/v11100955.

[50] G. Uchida, et al., Effects of nonthermal plasma jet irradiation on the selective production of h2o2 and no2− in liquid water, J. Appl. Phys. 120 (2016), https://doi.org/10.1063/1.4968568.

[51] L. Miebach, et al., Conductive gas plasma treatment augments tumor toxicity of ringer's lactate solutions in a model of peritoneal carcinomatosis, Antioxidants 11 (2022) 1439, https://doi.org/10.3390/antiox11081439.

[52] D. Yan, et al., Toward understanding the selective anticancer capacity of cold atmospheric plasma–a model based on aquaporins (review), Biointerphases 10 (2015), 040801, https://doi.org/10.1116/1.4938020.

[53] G. Bauer, Tumor cell-protective catalase as a novel target for rational therapeutic approaches based on specific intercellular ros signaling, Anticancer Res. 32 (2012) 2599–2624.

[54] J. Van der Paal, et al., How membrane lipids influence plasma delivery of reactive oxygen species into cells and subsequent DNA damage: an experimental and computational study, Phys. Chem. Chem. Phys. 21 (2019) 19327–19341, https://doi.org/10.1039/c9cp03520f.

[55] J. Van der Paal, et al., Effect of lipid peroxidation on membrane permeability of cancer and normal cells subjected to oxidative stress, Chem. Sci. 7 (2016) 489–498, https://doi.org/10.1039/c5sc02311d.

[56] S. Bekeschus, et al., Tumor cell metabolism correlates with resistance to gas plasma treatment: the evaluation of three dogmas, Free Radic. Biol. Med. 167 (2021) 12–28, https://doi.org/10.1016/j.freeradbiomed.2021.02.035.

[57] O. Lunov, et al., Chemically different non-thermal plasmas target distinct cell death pathways, Sci. Rep. 7 (2017) 600, https://doi.org/10.1038/s41598-017-00689-5.

[58] X. Dai, et al., Programmed cell death, redox imbalance, and cancer therapeutics, Apoptosis 26 (2021) 385–414, https://doi.org/10.1007/s10495-021-01682-0.

[59] D. Yan, et al., Multi-modal biological destruction by cold atmospheric plasma: capability and mechanism, Biomedicines 9 (2021), https://doi.org/10.3390/biomedicines9091259.

[60] G.E. Conway, et al., Non-thermal atmospheric plasma induces ros-independent cell death in u373mg glioma cells and augments the cytotoxicity of temozolomide, Br. J. Cancer 114 (2016) 435–443, https://doi.org/10.1038/bjc.2016.12.

[61] J.M. Vaquerizas, et al., A census of human transcription factors: function, expression and evolution, Nat. Rev. Genet. 10 (2009) 252–263, https://doi.org/10.1038/nrg2538.

[62] N. Nakamura, et al., Forkhead transcription factors are critical effectors of cell death and cell cycle arrest downstream of pten, Mol. Cell Biol. 20 (2000) 8969–8982, https://doi.org/10.1128/MCB.20.23.8969-8982.2000.

[63] A. Dhar, et al., The role of ap-1, nf-κb and ros/nos in skin carcinogenesis: the jb6 model is predictive, Mol. Cell. Biochem. 234/235 (2002) 185–193, https://doi.org/10.1023/a:1015948505117.

[64] G.S. Youn, et al., Overexpression of hdac6 induces pro-inflammatory responses by regulating ros-mapk-nf-kappab/ap-1 signaling pathways in macrophages, Free Radic. Biol. Med. 97 (2016) 14–23, https://doi.org/10.1016/j.freeradbiomed.2016.05.014.

[65] M. Vaeth, et al., Nfat control of immune function: new frontiers for an abiding trooper, F1000Res 7 (2018) 260, https://doi.org/10.12688/f1000research.13426.1.

[66] C. Huang, et al., Hydrogen peroxide mediates activation of nuclear factor of activated t cells (nfat) by nickel subsulfide, Cancer Res. 61 (2001) 8051–8057.

[67] X.M. Shi, et al., Low-temperature plasma promotes fibroblast proliferation in wound healing by ros-activated nf-kappab signaling pathway, Curr. Med. Sci. 38 (2018) 107–114, https://doi.org/10.1007/s11596-018-1853-x.

[68] B.K. Robbs, et al., The transcription factor nfat1 induces apoptosis through cooperation with ras/raf/mek/erk pathway and upregulation of tnf-alpha expression, Biochim. Biophys. Acta 1833 (2013) 2016–2028, https://doi.org/10.1016/j.bbamcr.2013.04.003.

[69] G.P. Mognol, et al., Cell cycle and apoptosis regulation by nfat transcription factors: new roles for an old player, Cell Death Dis. 7 (2016), e2199, https://doi.org/10.1038/cddis.2016.97.

[70] S.Y. Shin, et al., Coupled feedback regulation of nuclear factor of activated t-cells (nfat) modulates activation-induced cell death of t cells, Sci. Rep. 9 (2019), 10637, https://doi.org/10.1038/s41598-019-46592-z.

[71] C.V. Suschek, et al., The application of cold atmospheric plasma in medicine: the potential role of nitric oxide in plasma-induced effects, Clin. Plas. Med. 4 (2016) 1–8, https://doi.org/10.1016/j.cpme.2016.05.001.

[72] A. von Knethen, et al., Nf-kappab and ap-1 activation by nitric oxide attenuated apoptotic cell death in raw 264.7 macrophages, Mol. Biol. Cell 10 (1999) 361–372, https://doi.org/10.1091/mbc.10.2.361.